MULTIPLE INCIDENCE ANGLE SIR-B EXPERIMENT OVER ARGENTINA

JoBea Cimino, Daren Casey, and Stephen Wall
Jet Propulsion Laboratory
California Institute of Technology
Pasadena, California

Aldo Brandani
Consejo Nacional de Investigaciones Cientificas y Técnicas
and Centro de Geologia de Costas
Mar del Plata, Argentina

Gitta Domik and Franz Leberl
VEXCEL Corporation
Boulder, Colorado

I. INTRODUCTION

The Shuttle Imaging Radar (SIR-B), the second synthetic aperture radar (SAR) to fly aboard a shuttle, was launched on October 5, 1984. One of the primary goals of the SIR-B experiment was to use multiple incidence angle radar images to distinguish different terrain types through the use of their characteristic backscatter curves. This goal was accomplished in several locations including the Chubut Province of southern Argentina. Four descending image acquisitions were collected providing a multiple incidence angle image set. The data were first used to assess stereo-radargrammetric techniques (Leberl, et al., 1986a). A digital elevation model was produced using the optimum pair of multiple incidence angle images. This model was then used to determine the local incidence angle of each picture element to generate curves of relative brightness vs. incidence angle (Cimino, et al., 1986). Secondary image products were also generated using the multi-angle data (Domik, et al., 1986).

II. OBSERVATIONS

A. Acquired Data

The images examined in this study were acquired on consecutive days of the SIR-B mission with incidence angles from vertical of 33.0°, 44.7°, 53.7° and 59.4° (Figure 1 and Table 1). The center latitude and longitude of the site are 43°20'S and 71° 27'W, respectively, near a peak named Cordón la Grasa. The images were collected at about 6 p.m. local time between October 8 and 11, 1984. The width of the area of coincident coverage ranges from about 12 to 15 km.

B. Description of the Study Area

The majority of the study area imaged by SIR-B is within a sharp boundary controlled by a strong east-west rainfall gradient which divides the Andes ecosystems from the Patagonian desert. The ecotone includes plant species from the Andean forests and from the Patagonian steppe (Figure 1b). The study area encompasses the Valle Rio Frio and the terrain just east and

west of it. Cordón la Grasa, one of the series of ranges forming the Andes Pre-Cordillera, dominates the western portion of the image. A pure Nothofagus pumilio, or lenga, forest is found at higher elevations and along water courses. Below the lenga to the Valle Rio Frio, there is a complex unit formed by both pure Nothofagus antarctica, or ñire, forest between 1000 m and 1050 m elevation, and ñire mixed with maiten (Maytenus boaria), laura (Schinus patagonicus) and several species of Berberis below 1000 m. Locally, the ratio of ñire, maiten, laura and berberis varies depending on slope, exposure, and available moisture. The ecosystems are described in detail by Cimino, et al., 1986.

III. ANALYSIS OF THE IMAGERY

A. Radargrammetric Analysis

The multiple incidence angle data set permits one to study the capabilities and limitations of radargrammetric mapping in a manner previously not possible due to a lack of available data. Figure 2(a) is a sketch of the imaging configurations. The largest intersection angle for stereoscopic analysis was 23 degrees (Table 2). This stereo model may present a different quality of stereo-viewing than one using data with smaller intersection angles. Generally one can expect the best visual stereo-matching when the intersection angles are at a minimum. Unfortunately, however, this would lead to poor vertical exaggeration of the stereo-model.

The radargrammetric measurements and computations were performed on a computer-controlled photogrammetric analytical stereo-plotter. The analysis procedure consists of several steps:

- Ground control points are identified on existing topographic maps and in each of the 6 pairs of overlapping radar images;
- On the computer-controlled stereo instrument, 18 different stereo models were set-up and measurements of coordinates were taken;
- A digital contour map was created from the most accurate of the radar stereo models;
- A reference digital elevation matrix was obtained using the maps of the study area; and
- The radar- and map-derived digital elevation data were compared.

Figure 2(b) illustrates graphically the results of the comparison in terms of the change in accuracy as a function of stereo-intersection angle. The results at a 5° intersection are nearly as predicted; at 23° the experimental data are poorer than those expected. Figure 2(b) is based on the Cordón la Grasa data set and on results from another SIR-B multiple angle data set of Mt. Shasta (Leberl et al., 1986b).

It is evident that height values are less accurate than theoretical prediction based on range resolution. This difference becomes more distinct as stereo-intersection angles increase. Limitations in accuracy at large intersection angles may be due to

- effects of "specular point migration" and migration of edges due to differences in illumination;

- changes in backscatter due to differences in incidence angles;
- variations in radar azimuth angle and resulting edge migration;
- effects of noise.

B. Generation of Color Composite Image

To assess visually the value of a multiincidence angle image set over that of a single image for vegetation classification, a color composite was generated using three of the four SIR-B images. Registered, geometrically corrected digital images (Domik, et al., 1986) from three of the four acquisitions of the Cordón la Grasa area were used to produce the color composite by assigning each image a color. The 33.0° incidence angle image was assigned to a blue color, the 44.7° image to a green and the 59.4° image to red. The composite (see Cimino, et al., 1986) clearly delineates the forest units which may be discriminated when the multiple incidence angle data sets are combined.

C. Generation of Relative Brightness Curves

Although SIR-B was designed as a calibrated system, images in the resulting data set resist quantitative interpretation because of an unexpected breakdown in the insulation of the cabling connecting the transmitter/receiver unit to the antenna during the flight. The effect of the breakdown was to modulate the effective antenna gain; the frequency spectrum of this modulation is unknown. However, short term variations in azimuth are strongly damped by the correlation process, which effectively averages returned echoes over a 2-second interval. Such averaging insures that comparisons of data separated by 15 km or less are legitimate.

Day-to-day variations in transmitted power are compensated by the use of ratios--that is, all multiple-angle data are presented in terms of brightness relative to a reference forest unit.

For selected forest units, several areas uniform in image brightness were chosen for analysis (Figure 3a). The digital values or data numbers (DN) of the pixels in each box were averaged to remove speckle. The averages were corrected for all known receiver and processing gain variations and plotted as a function of local incidence angle using topographic information generated by Leberl, et al., 1986a. The curves for each vegetation type were then ratioed to the low ñire forest curve (unit 8). Error bars are the root-sum-square of the speckle noise and the overall relative calibration error (SIR-B Science Plan). In general, the overall relative calibration error dominates.

IV. RESULTS AND DISCUSSION

The resulting curves of relative brightness vs incidence angle (Figure 3b) describe in a more quantitative fashion the results displayed in the color composite. The lenga forest has a significantly stronger response at the smaller incidence angles than the surrounding ñire forest. At 59°, the curves of the lenga and the ñire forests on the west side of Cordón la Grasa

converge. The lenga in the Andes also has a much stronger response than the nire but a slightly weaker response than the lenga on Cordón la Grasa.

The ñire forests on the east and west sides of Cordón la Grasa have very similar responses at the three smallest incidence angles. The regenerated ñire (unit 3) has a slightly lower response than the other ñire forests. At the largest incidence angle, however, the ñire on the west side of Cordón la Grasa have a much stronger response than the low ñire forests (unit 8) on the east side. The wind damaged ñire (unit 7) has a response similar to the low ñire. The grazed mallines have a much lower response at all three larger incidence angles than the forests, however at the smallest incidence angle, their responses are similar to the regenerated ñire. The bare rocks and snow at the peak of Cordón la Grasa have the weakest response at all incidence angles.

At the smallest incidence angle the lenga forest has the strongest backscattered return. The relative openness of the canopy suggests that a significant amount of radiation is reaching the surface. The extreme brightness may be due to a high density of trees and branches littering the ground below the canopy. For the horizontally polarized radar these horizontal branches are likely to be very good scatterers. At higher incidence angles the incident radar beam must penetrate increasingly greater amounts of canopy before breaking through to the understory, until at the highest incidence angle little radiation reaches the surface and the lenga backscatter is reduced to that of the ñire. The branching structures of the lenga and ñire tree canopies are very similar, and in situations where most of the radiation is either scattered or absorbed within the upper levels of the canopies, such as at 59°, it is reasonable to assume these two forests look the same to the radar.

The ñire forests have a wide variety of structures depending on the elevation, exposure to the sun and wind and the stage of regeneration if burning has occurred. The shrub-like ñire (unit 8) is a weaker scatterer than the tree-like ñire at the largest incidence angle. A possible explanation for this relatively low backscatter is that the canopy is so dense that it scatters like a smooth surface. At other incidence angles the two types of ñire have essentially the same brightness.

The results of this work indicate that (1) various forest species and various structures of a single species may be discriminated using multiple incidence angle radar imagery and (2) it is essential to consider the variation in backscatter due to a variable incidence angle when analyzing and comparing data collected at varying frequencies and polarizations.

ACKNOWLEDGEMENTS

The work described in this paper was carried out under contract with the National Aeronautics and Space Administration at the Jet Propulsion Laboratory, California Institute of Technology.

REFERENCES

Cimino, J., A. Brandani, D. Casey, J. Rabassa, and S. Wall, 1986, "III. Multiple Incidence Angle SIR-B Data over Argentina: Mapping of Vegetation Units," IEEE, July issue.

Domik, G., F. Leberl and J. B. Cimino, 1986, II. Multiple Incidence Angle SIR-B Experiment Over Argentina: Generation of Secondary Image Products, IEEE, July issue.

Leberl, F., G. Domik, J. Raggams, J. Cimino, M. Kobrick, 1986a, I. Multiple Incidence Angle SIR-B Experiment Over Argentina: Stereo-Radargrammetric Analysis, IEEE, July issue.

Leberl, F., J. Raggam, G. Domik, M. Kobrick, 1986b, "Radar Stereo Mapping Techniques and Application to SIR-B Images at Mt. Shasta, IEEE, July issue.

SIR-B Science Plan, 1984, JPL Publication 82-78, Pasadena, CA.

Table 1. Multiple incidence angle SIR-B data set

Data take	Center incidence angle	Date (1984)	On GMT	Duration (min)	Azimuth look direction
56.4	33.0°	Oct. 8	282/22:31:0	4	N42E
72.4	44.7°	Oct. 9	283/22:14:0	2	N40E
88.4	53.7°	Oct. 10	284/21:57:0	2	N40E
104.4	59.4°	Oct. 11	285/21:39:0	4	N39E

Table 2. Intersection angles

Case	Data takes	Look angles	Intersection angles
I	104/88	56°/51°	5°
II	88/72	51°/43°	8°
III	72/56	43°/33°	10°
IV	104/72	56°/43°	13°
V	88/56	51°/33°	18°
VI	104/56	56°/33°	23°

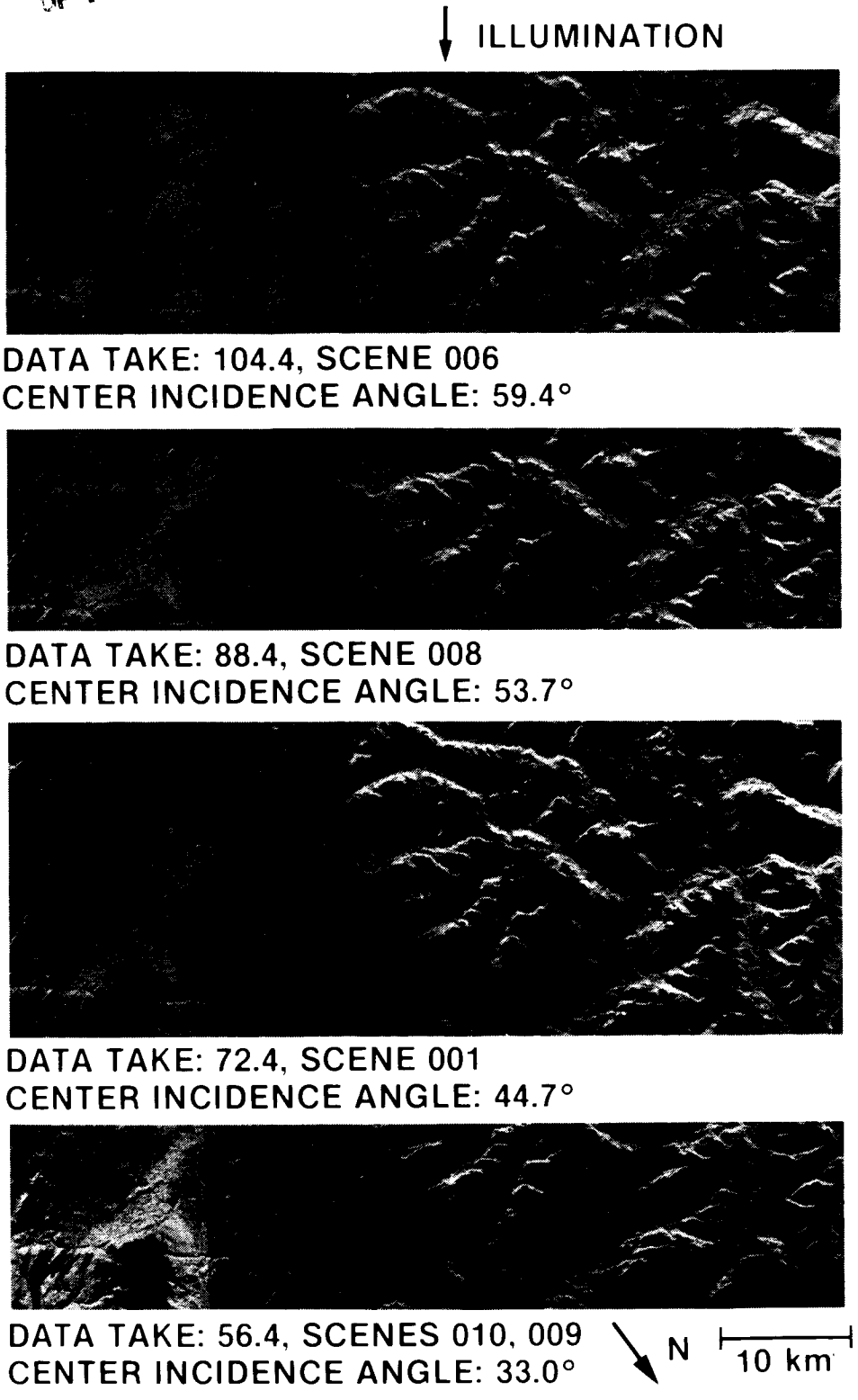

Figure 1a. The four multiple incidence angle images of the Cordón la Grasa region.

SIR-B/ARGENTINA
MAP OF ECO-GEOMORPHOLOGIC UNITS

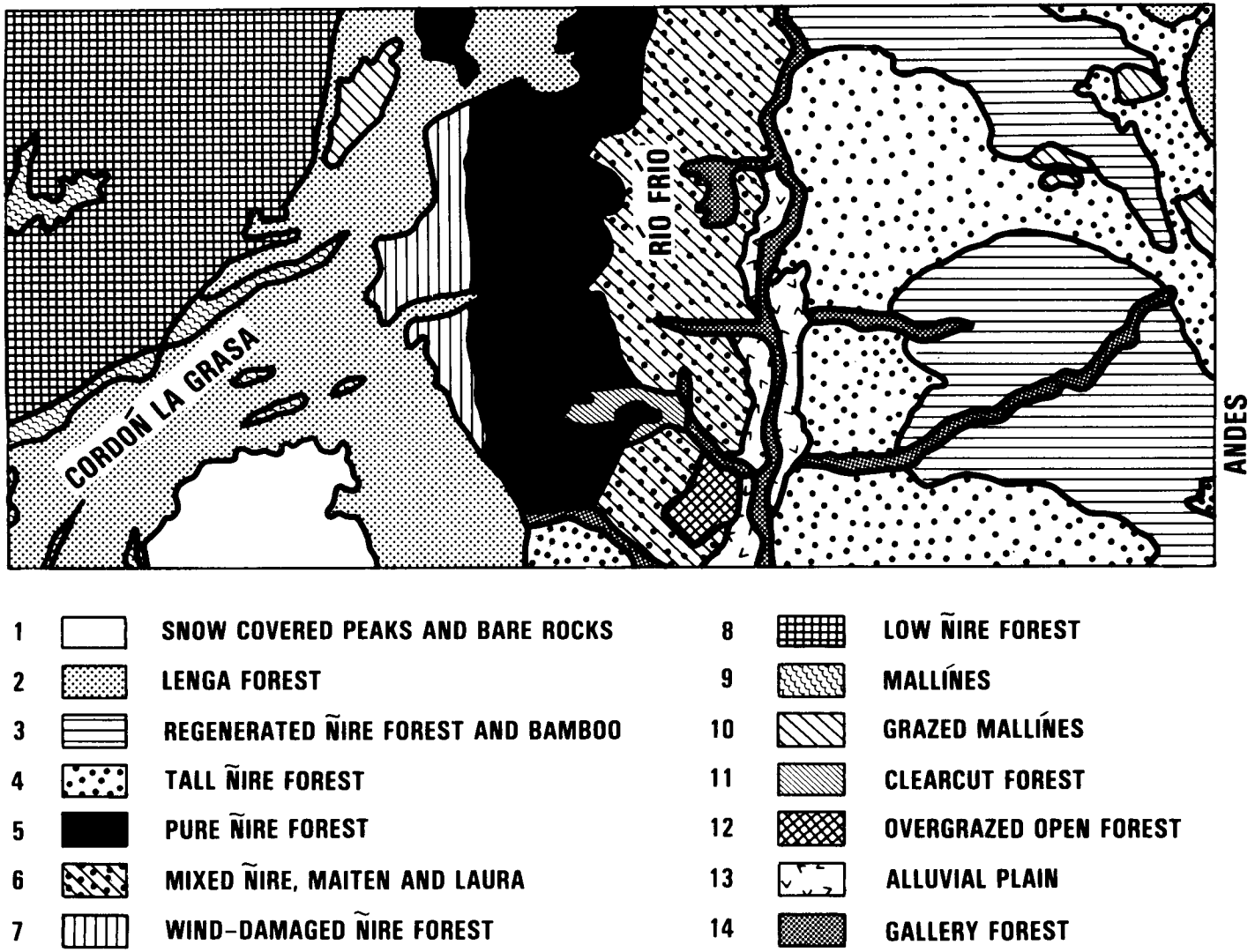

Figure 1b. Vegetation map of the Cordón la Grasa region.

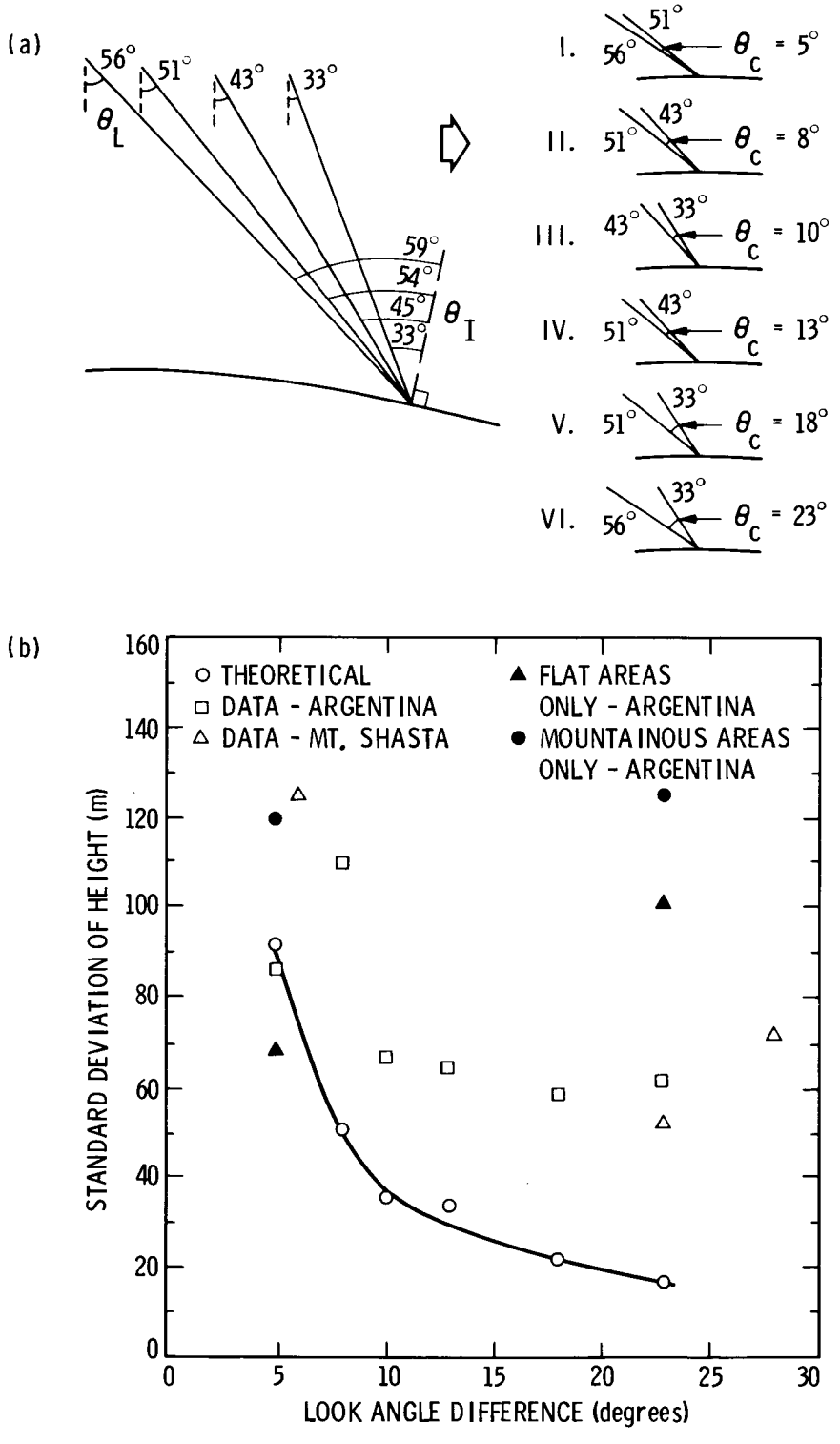

Figure 2. (a) Look angle geometry of 6 stereo models formed by the 4 images of Figure 1a; (b) Height accuracy versus stereo intersection angles, both as predicted and obtained experimentally.

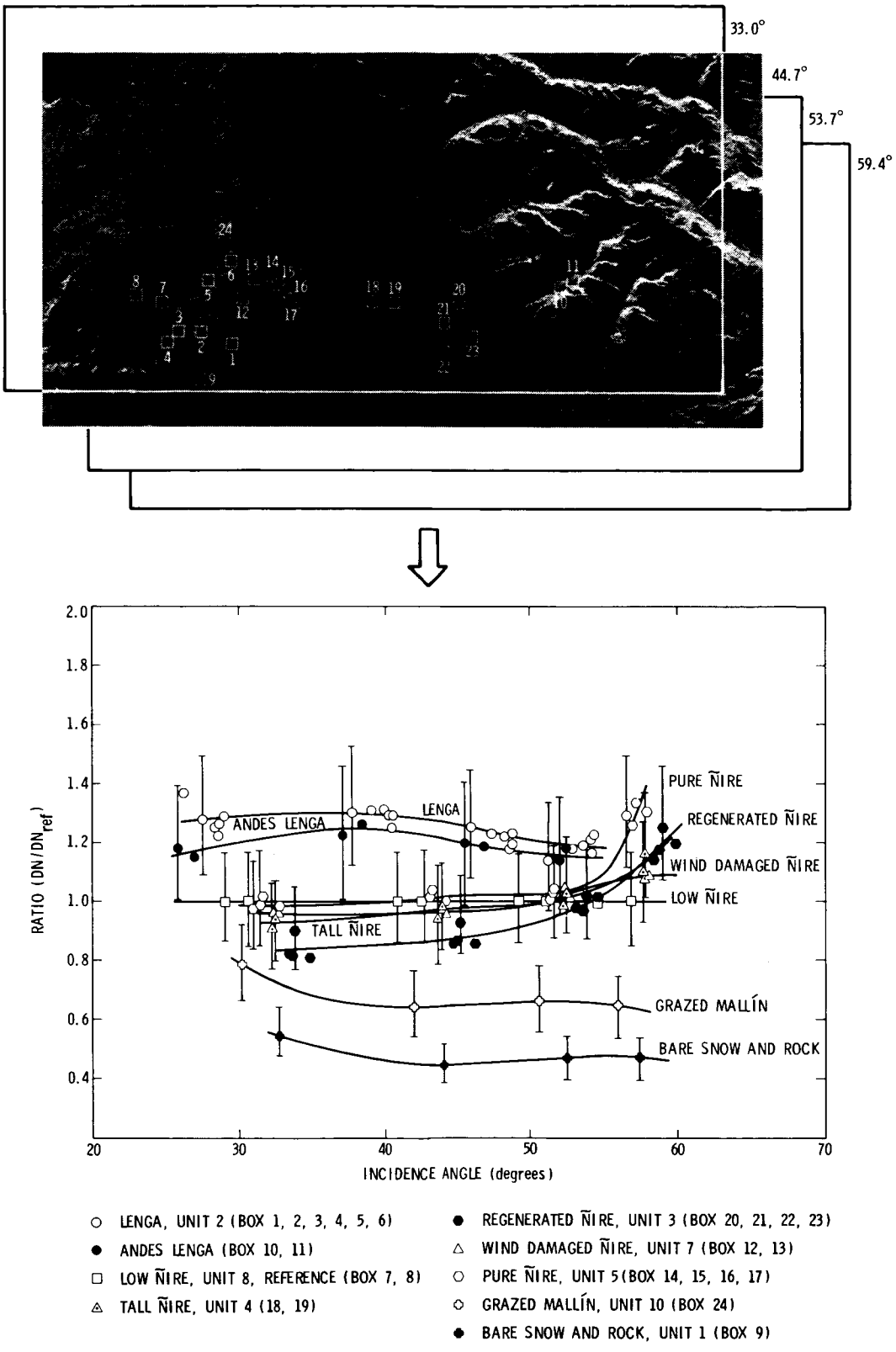

Figure 3. (a) SIR-B image showing location of areas used to generate relative brightness curves; (b) Relative brightness as a function of local incidence angle.

C-3